Caving 2022 - Y Potvin (ed.)

doi:10.36487/ACG_repo/2205_44

X-ray computer tomography and ground conditions at Northparkes cave edges to further the understanding of the caving mechanisms of strain and hydraulic conductivity

S Webster *CMOC Northparkes, Australia*

L Snyman *CMOC Northparkes, Australia*

N Francois *The Australian National University, Australia*

M Saadatfar *The Australian National University, Australia*

Abstract

It is generally understood that rock mass strain increases from the intact, undisturbed zone towards a block cave edge damaged region and into the mobilised zone. The ability to observe this underground is restricted by a lack of safe observation points. However, from this information, the current understanding of cave growth is commonly described using the Duplancic & Brady (1999) caving model. Here, ground conditions transition from pseudo-continuous intact rock to seismogenic, degraded, and loosened rock, and finally, rock mobilised within the cave. The characteristics of the damaged cave zones are highly variable and impact the ongoing caveability, nearby mining activities and hydraulic conductivity.

Numerical models can now model these pieces by coupling the interactions of the cave muck pile particle flow, geomechanical response to caving, and hydrological effects. The relationship between each of the components is non-linear and in terms of the hydrology, more definition is required. To improve the efficacy of the hydrological models, the authors are undertaking an experimental project to better define the relationship between hydrological properties and strain. The first triaxial experiment has been performed on the E26 core coupled with X-ray microcomputer tomography (XCT) imaging throughout the loading stages. The images presented here enable 3D visualisation of the complex failure mechanisms and the relationship between strain, fracture dilation, and fracture connectivity.

At the same time, Northparkes has mined adjacent and into historic block caves where the development mines against the existing cave edge and in some instances, exposed the mobile caved zone. This allowed observations of the ground conditions transitioning from the pseudo-continuous intact ground through to the mobilised zone and the failure mechanisms encountered.

This paper presents underground observations of the variable failure mechanisms encountered from the cave operations. These observations are reconciled against the geomechanical model results to show how strain presents in the mine. The modelling, failure mechanisms, and experiment imaging are brought together to better illustrate the coupling and non-linear relationship between strain, fracture mechanics, and hydraulic conductivity.

Keywords: *failure mechanism, strain, permeability, field observations*

1 Introduction

The caveability of an orebody is a relationship between the rock mass strength, structure, strain, stress, hydrology, geometry, and draw. A caving study aims to predict the cave failure timing, rate of propagation, extents of the cave and any areas requiring preconditioning treatment. History shows that for numerous reasons, including variable geological conditions, draw strategies and simplified modelling, cave predictions deviate from final cave results. Interpretations of caveability refer to Duplancic & Brady's (1999) conceptual

model (Figure 1) that presents increasing damage zones from intact rock towards the cave, consisting of five main zones:

- Pseudo-continuous, elastic domain.
- Seismogenic zone.
- Zone of loosening or yielded zone.
- Airgap.
- Mobilised zone.

The zones in practice are of changing thickness and present in various ways depending on the rock mass, stress, and strain. Additionally, the influence of the airgap and caved zone on the material at the cave edge is significant and now captured through coupled flow and mechanical modelling.

The consideration of hydrology into a stability model is known to be important however is often not performed due to limitations in modelling. Additionally, hydrology modelling is more commonly performed in porous media, for example, sandstone aquifers. In hard rock settings, most groundwater movement occurs in joints and fractures with volcanic and intrusive rocks typically exhibiting only fracture flow (Read & Stacey 2009). Open fractures tend to have a higher permeability compared to an equivalent porous media. Furthermore, fractures increase with damage as Bieniawaski (1967) defined in the stages of brittle rock failure are as crack closure, fracture initiation, stable fracture propagation, unstable fracture propagation and strength failure, coalescence of cracks, and rupture. The relationship between fracture dilation, conductivity, damage and stress is complex and observed as mining areas transition through stress conditions.

A coupled modelling solution for cave flow, mechanical and hydrological properties is outlined by Flatten et al. (2016). In this coupling scheme, the mechanical response of the rock and discontinuities, movements in the muck pile and regional and local effects of porewater pressure changes due to mining and dewatering are solved. The conceptual image of the cave zones, and the discontinuities and damage zones that impact the conductivity are shown in Figure 2.

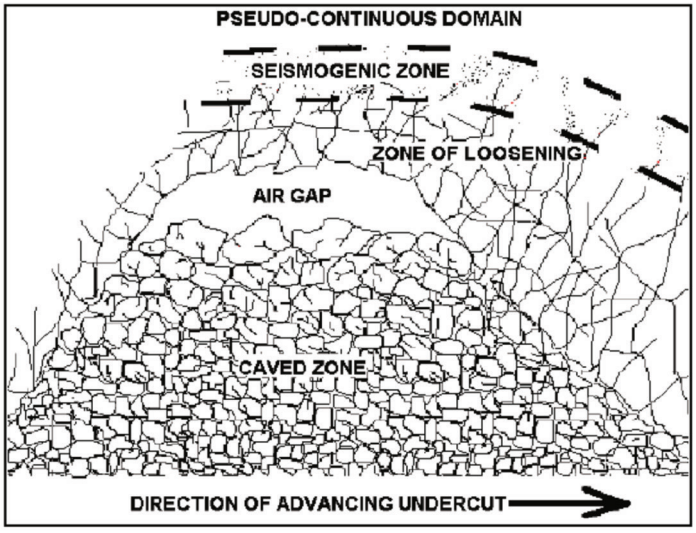

Figure 1 Main zones of a propagating cave (Duplancic & Brady 1999)

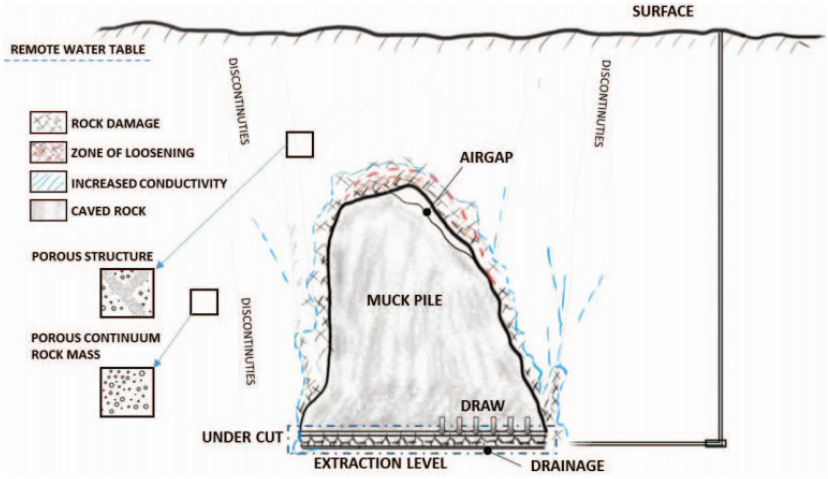

Figure 2 Conceptual representation of the block cave model highlighting the different porous elements relative to the cave (Flatten et al. 2016)

During cave propagation, there are limited opportunities to directly observe cave zones and the failure mechanisms as information is taken from borehole observations and inferred from various monitoring systems.

Umar (2017) performed numerical simulations based on mapping and field observations at LKAB mines and observed that shear failure was dominant in the cap rock and tensile failure dominant in the hanging wall and close to the cave. Furthermore, the estimated cave zones of seismogenic and yielded zones were close to the caving boundary in the Printzsköld orebody studied, implying that the yielded zone was not present in some areas.

Northparkes has mined three block caves with different caveability challenges and results (Talu et al. 2010; Ross & van As 2005). In the last 10 years block cave and sublevel cave extensions have been constructed where development has mined up against the cave, leaving no pillar between the new and old cave (Webster et.al., 2020). During the study stages, coupled mechanical and flow modelling is performed to understand and improve cave performance and manage risks. The models show strain values that indicate damage to the excavations and how this materialises can be misunderstood. Small-scale structure is considered with the rock mass properties within the models and is homogenised within the model representative volume element (RVE). Model results can also appear smeared across the RVE and visually correlating the results to a fractured medium is helpful to communicate and reinforce the modelled appearance on the excavation. Development through the cave edges has provided the opportunity to study the rock mass surrounding the E26 cave and share how the ground conditions present. The visual evidence for air and water conductivity changes through the rock can also be observed through mineral oxidation on surfaces and water staining.

The relationships between the coupled models are non-linear and the mathematical relationship between hydraulic conductivity and strain has not been directly measured in heterogenous hard rock. Therefore, Northparkes rocks are being used in an experimental study to measure permeability and strain. The first triaxial experiment has been performed with nine X-ray microcomputer tomography (XCT) images collected throughout the loading stages. The images enable 3D visualisation of the complex failure mechanisms of the heterogenous sample showing fracture dilation and fracture connectivity at progressive stages of strain. Strain focused on discontinuities within the XCT and cave edges are comparable and provide observations for changes to the hydraulic conductivity with damage.

2 Northparkes cave edge mining overview

Northparkes have mined three block caves in the E26 porphyry system. This has included two extensions that mine up against the cave edge in the last five years. The location of these two mines, the E26 sublevel cave and the E26 Lift 1 North Block Cave, is shown in Figure 3. These mines target the halo and under broken cave mineralisation surrounding the original cave mines.

The E26 rock mass contains three orthogonal joint sets along with other minor joints. The host rocks at E26 are strong with median uniaxial compressive strength 120 MPa in the monzonite and 118 MPa in the volcanics. The median Young's modulus is 53 GPa in the monzonite and 56 GPa in the volcanics and rock mass rating averages 76–77 for both units. At the extension depth of 500 m the major principal stress is horizontal 29 MPa, intermediate stress 15 MPa and minor stress is 12 MPa and vertical.

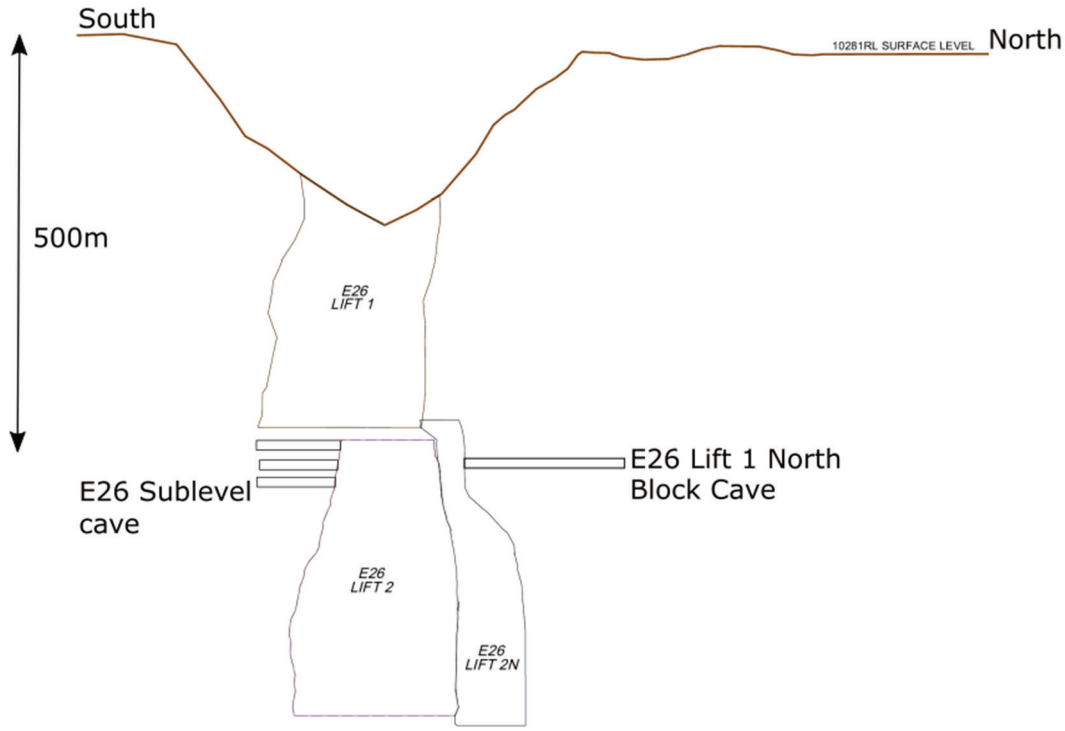

Figure 3 Cross-section through E26 caves Lift 1, Lift 2 and Lift 2 North with locations of cave edge mining at E26 sublevel cave and E26 Lift 1 North Block Cave

The E26 sublevel cave (SLC) was mined as the first extension to E26, with four of the six planned levels completed. This SLC was located south and west of the Lift 2 cave (Figure 4), in a wedge of ore reserves remaining due to the underbreak of the E26 Lift 2 cave. The E26 Lift 1 North Block Cave (E26L1N) is located North and East of the Lift 2 cave, in halo and adjacent porphyry mineralisation (Figure 5). Both caves mined development drives towards the edge of the Lift 2 cave with the plan to fire the sublevel cave rings and the block cave undercut rings against the cave edge to break into the cave. The drives were designed to not break through to the cave due to the uncertainty of containing the mobilised cave material during the task of uphole ring drilling and charging. However, there were examples when the development broke through to the cave and the cave edge and mobilised zone could be observed.

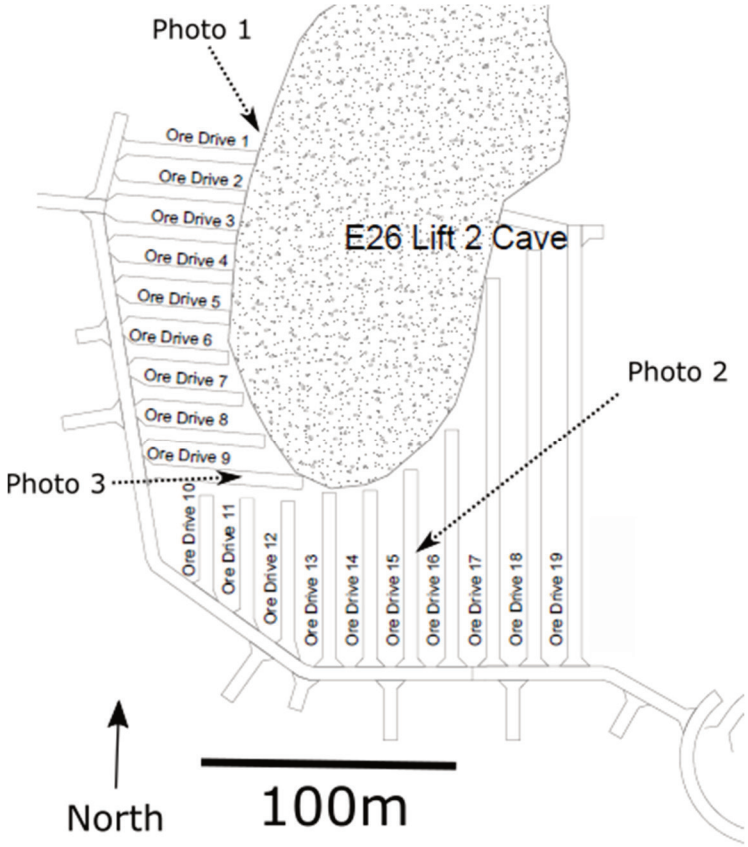

Figure 4 **Plan view of E26 sublevel cave, level 4, RL9640, showing the drives mined against the E26 Lift 2 cave. Photo locations refer to SLC photos in the paper**

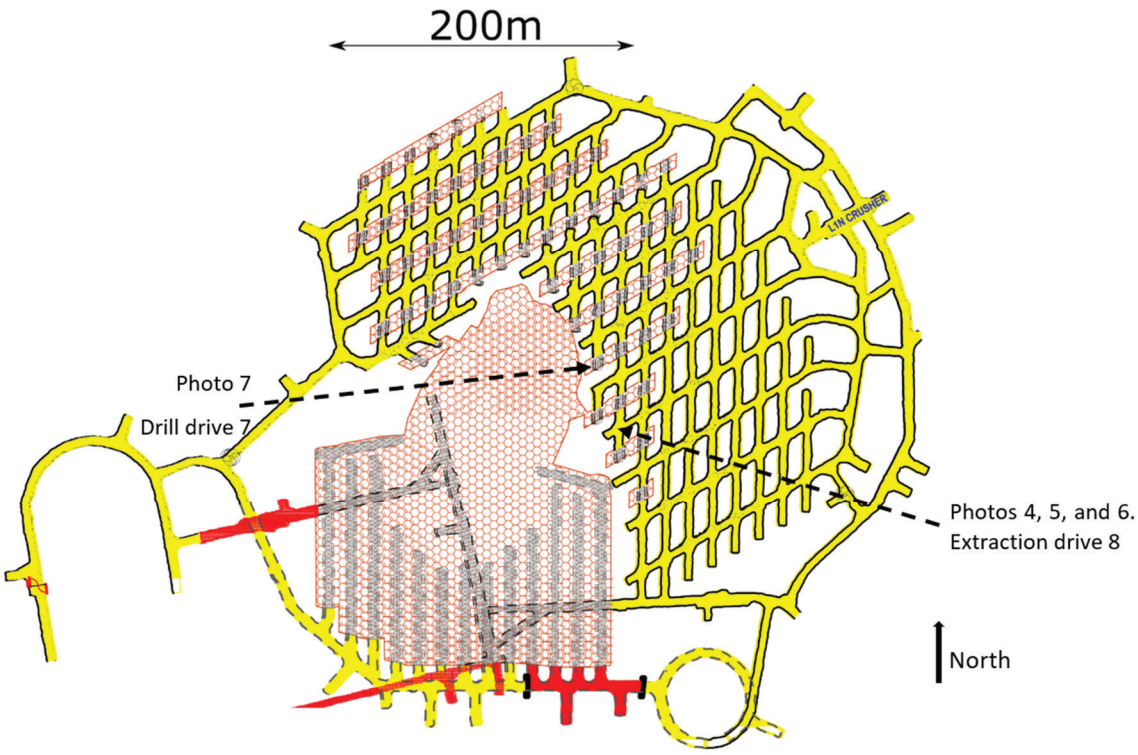

Figure 5 **Plan view of E26 Lift 1 North Block Cave, showing the RL9760 extraction level and RL9780 undercut level drives mined against the E26 Lift 2 cave**

Mine stability and caveability modelling performed for the SLC and block caves indicated the cave edges are in a relaxed, destressed state as shown in the blue regions of the section view of sigma 1 in Figure 6. The sublevel cave is also located in the stress shadow from the remnant Lift 1 footprint above. During development, damaging seismicity was not common in these mines. When rings were fired in the SLC and retreated from the destressed cave edge to the access areas, seismicity increased away from the cave and with increasing SLC depths (Figure 6). A similar pattern was encountered in the block cave where seismicity was measured closer to the access drives than the cave edges.

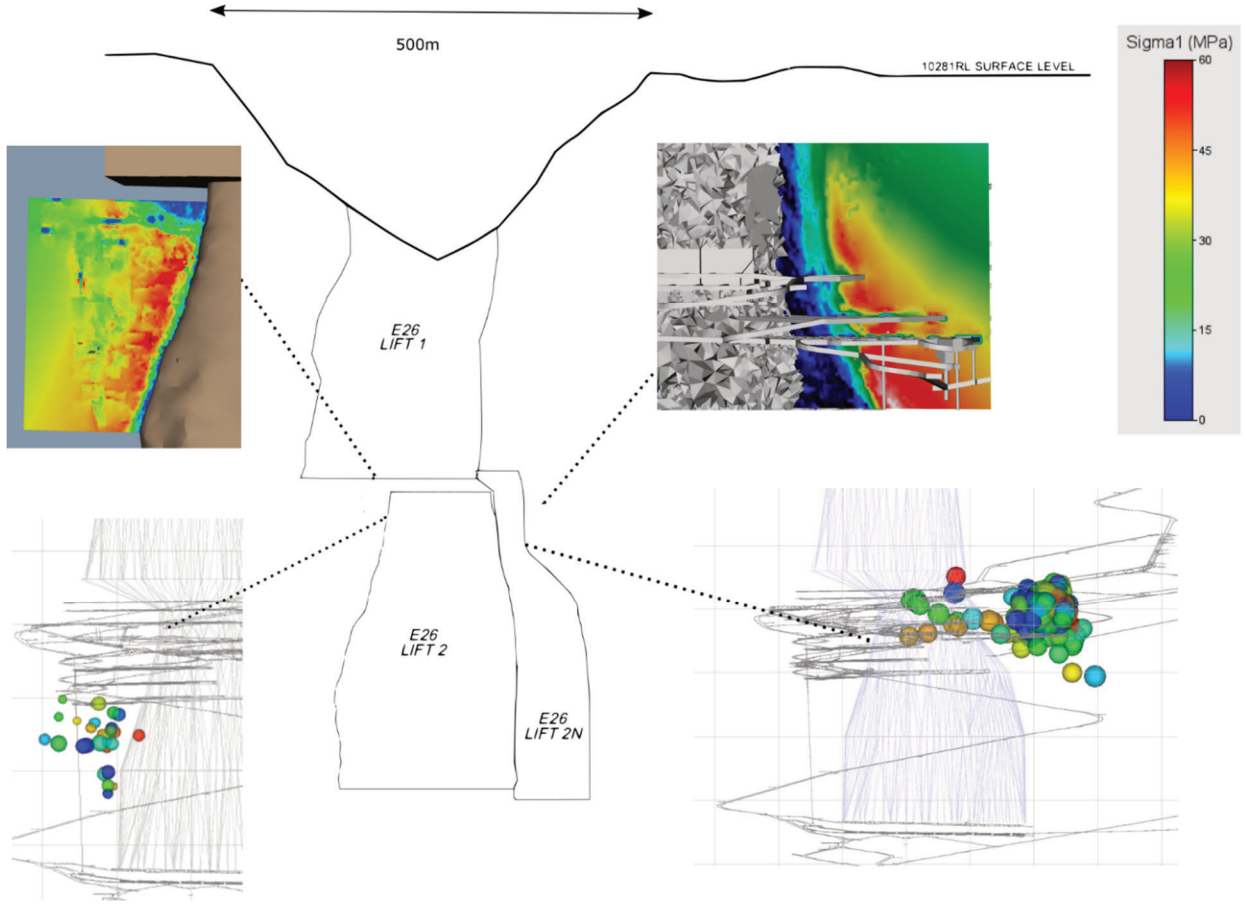

Figure 6 Locations of cave edge stress modelling and one week of localised seismicity during SLC and E26L1N extensions. The E26L1N seismicity wraps around the footprint and events shown in 2D within the cave volume are west and east of the remnant cave

2.1 Types and locations of data

This section presents the direct observations of development headings and drill holes as they approach and break through the cave. The development observations adjacent to the cave edge were from sublevel cave drives, block cave extraction level drives, and undercut drives. Drilling into the cave provided a diamond drillcore of the rock mass adjacent to the cave and cave material. In addition, it allowed monitoring of the open holes and the cave breakthrough with borehole cameras. The locations of these holes and summary images are shown in Figure 7.

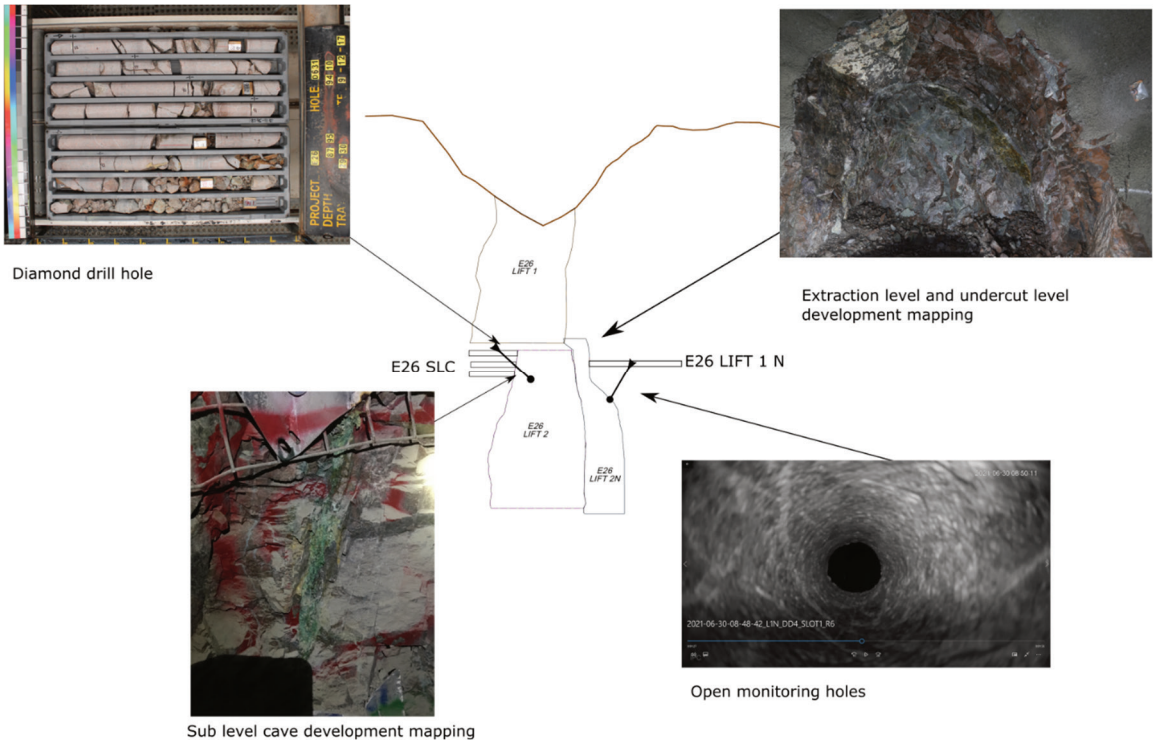

Figure 7 Section view of E26 cave showing the locations of data collected for this paper

2.2 Cave edge diamond drilling

Diamond drilling was performed through the lower levels of the sublevel cave to improve information on:

- Lower level reserves.
- Cave edge location and ground conditions.
- Impacts of previous preconditioning programs.
- Mobilised cave material dilution grade.
- Mobilised cave material clay content.

The drilling conditions were challenging as water return to the drill was at risk of being lost along with the drill bit into the cave. Due to this risk, only two holes were successfully drilled past the cave edge to recover mobilised cave material. The core trays from these holes are shown in Figure 8 (hole identification E26D631) and Figure 9 (hole identification E26D616).

The boundary between the cave edge is interpreted as the change in core recovery from intact core to rounded blocks of mixed lithology and alteration. The fine component from the mobilised zone of the cave was washed away and not able to be recovered with the drilling methodology. The recovered core and rubble showed a stepped increase in copper and gold grade compared to the cave wall grade. Natural fracture surfaces are oxidised in the 2 m before the cave boundary, where surfaces were sufficiently open for air and water to permeate them, indicating increased conductivity around the cave edges.

Hole E26D631 contains fresh fracture surfaces and these are interpreted as stress fracturing from the cave abutment. This type of fracture is evidence of stress fracturing and may be attributed to cave stress or blast preconditioning through the area that was conducted to promote caving. These ground conditions were identified as being problematic for development and production ring firings and additional ground support designed for the areas.

Hole E26D616 contains lengths of intact core adjacent to the cave edge, with no signs of fresh fracture surfaces. This wet core image clearly shows the range of rock types and concrete recovered from the mobilised cave zone.

Figure 8 Core tray of diamond drillhole E26D631 with recovered cave edge and mobilised cave material. The boundary between the two zones is interpreted to be at 93.4 m downhole. The last 0.7 m of material recovered is from the cave

Figure 9 Core tray of diamond drillhole E26D616 with recovered cave edge and mobilised cave material. The boundary between the two zones is interpreted to be at 31.5 m downhole. The end of the hole is at 33.4 m with partial recovery of mobilised rock within the cave

2.3 Open hole monitoring

Open monitoring holes are drilled from a safe location underground or on-surface through the orebody into the cave. They are used to deploy a borehole camera to observe the transition from intact, solid ground through the cave edge, the airgap, and if conditions are favourable, the muck pile below. The hole in Figure 10 has been drilled into the inactive E26 cave. In this area, the cave edge is observed as intact, solid ground with little rock loosening. The observations show dislocations but not gradational loosening of the rock mass back from the cave edge.

Figure 10 Image from borehole camera monitoring within undercut drill drive four in E26L1N block cave into the cave edge

2.4 Sublevel cave ore drives

E26 sublevel cave ore drives were mined perpendicular to the cave edge (Figure 4) and designed to stop short rather than breaking the drive through to the mobilised material. The end of drive conditions were anticipated to be loosened, and additional ground support in the form of shotcrete, mesh and resin bolts were installed. Cable bolts through the last 10 m of development before the cave were budgeted but deemed unnecessary for single drives as no loosened zone was encountered at the cave edge. However, cable bolts were installed to ensure ground support back from the cave edge, in the seismogenic zone, was sufficient for dynamic conditions.

An example where the cave edge was mined through is shown in Figure 11. Within this area, the mobilised, older cave material is partially oxidised within the cave and mixed with surface clays. In this area, blasting was performed to the cave edge then the cave edge was partially exposed with mechanical scaling of the face.

Mapping and observations of the sublevel cave ore drives showed a pattern of intact, blocky rock mass throughout the length of the drive towards the cave. Joints and minor scale faults were typically tight with intermittent discontinuities open (Figure 12a). These open structures were observed up to 50 m back from the cave edge. The orientation of open joints was not uniformly parallel to the cave edge, with open structures at times at an oblique angle to the cave edge, dipping both towards and away from the cave. Open joints were never observed perpendicular to the cave edge. When joints and faults were open, there was often evidence of surface oxidation and groundwater with little movement either side of the opening. Figure 12b shows a structure that has secondary oxide–copper mineralisation from groundwater. The condition of this structure is not common within the drive indicating groundwater movement and weathering were focused within individual structures rather than through an anastomosing network.

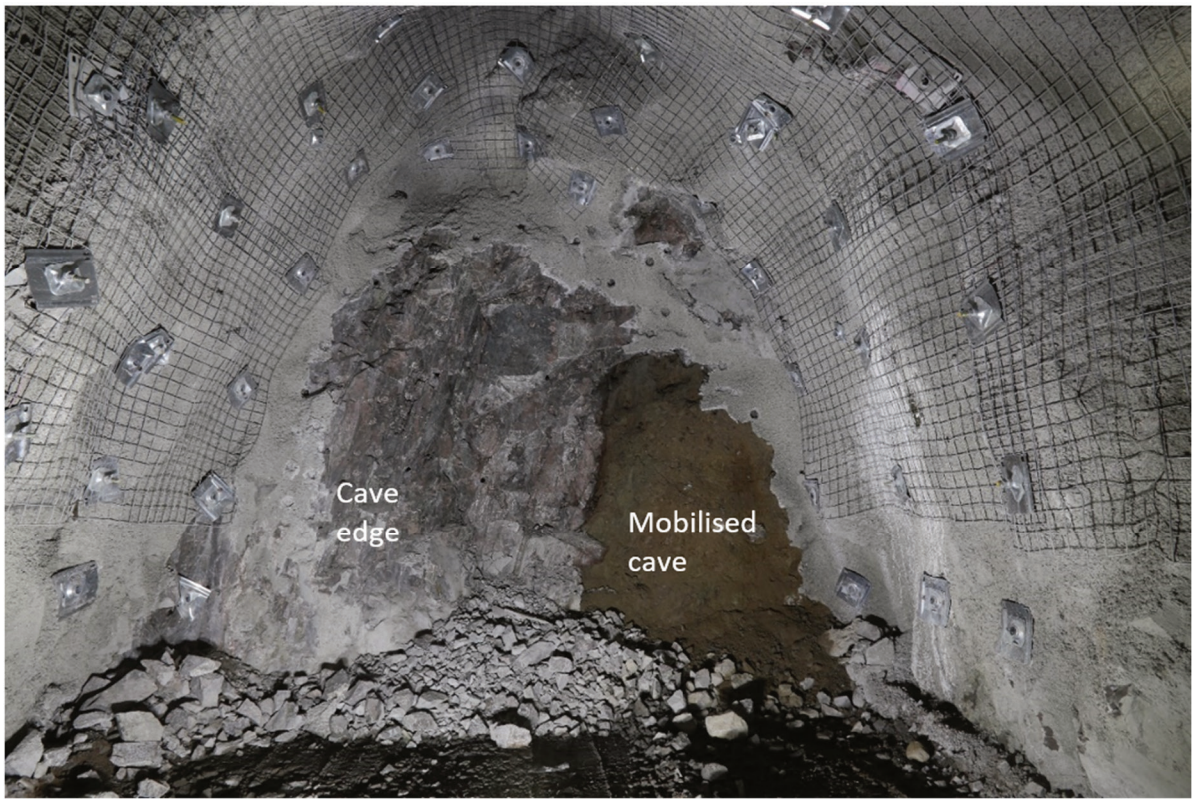

Figure 11 **Sublevel cave 9720 level, west slot drive showing the face partially broken through to the mobilised cave material. Note the scaling bit marks on the face and fibrecrete where loose material has been removed and the increased ground support installed. Photo 1 in reference location Figure 4**

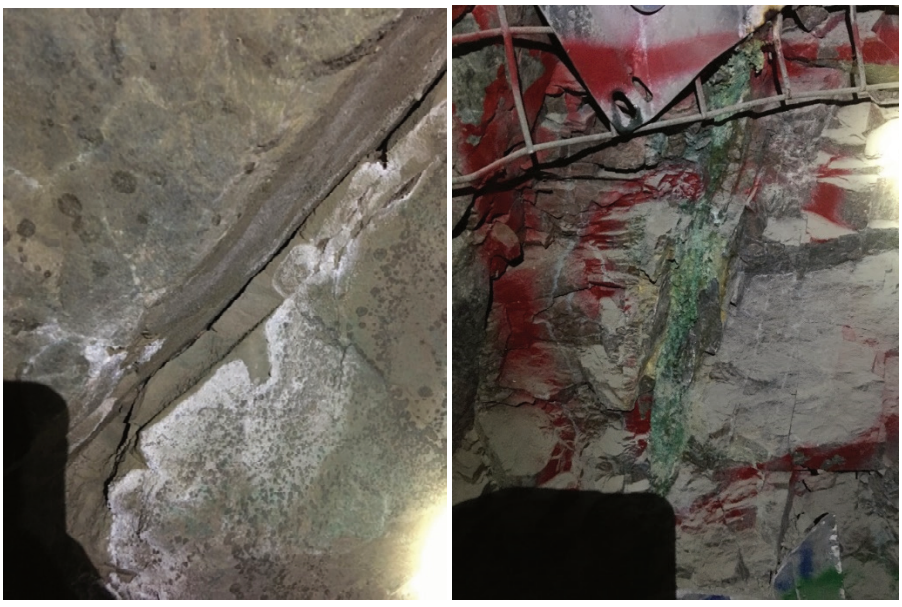

(a) (b)

Figure 12 **(a) Sublevel cave 9670 level, oredrive 15 showing an open joint approximately 50 m back from the interpreted cave edge. This oredrive strikes north–south and the joint dips 50° to 240° northwest dip direction. Photo 2 in reference location Figure 4; (b) Structure that has secondary oxide copper mineralisation from groundwater. This structure is from oredrive 9 striking east–west and dips 70° to 310°. The cave is to the right in both of these photos. Photo 3 in reference location Figure 4**

2.5 Block cave undercut and extraction drives

The E26L1N block cave was designed to mine perpendicular to the cave edge; however, there is less flexibility with the drive orientations compared to the SLC and one drive had to mine parallel to the cave. During development, similar good ground conditions to the SLC were encountered with intermittent oxidised surfaces approaching the cave edge (Figure 14b). In addition, the drive that was mined parallel to the cave edge contained damaged ground where open drill holes were difficult to maintain for use.

A localised portion of the E26L1N footprint, like the SLC, has experienced blasting preconditioning in the past to promote caveability. However, the northern side of the cave has the Lift 2 North cave beneath the extraction level; this portion of the cave stalled during propagation and is filled with cave material below the stalled area. Modelling of the extraction level stability indicated that regions with preconditioning and at the cave edges would experience damage to levels, resulting in them being unusable.

At the time of writing, the cave edge areas remain stable however, growing evidence of movement and damage is seen in the E26L1N cave during cave establishment. Within this area, en echelon shearing indications of downward movement are seen in the extraction drive end, some 10 m from the cave boundary (Figure 13a). These shears follow the orientation of the structural fabric seen in the ground leading up to the edge (Figure 13b). Like the diamond core into the cave edge, natural joints and faults are oxidised, indicating higher conductivity at cave edges due to strain on discontinuities. This downwards shear pattern was replicated in the undercut drive above (Figure 14a).

(a) (b)

Figure 13 (a) Shear cracks in extraction drive 8, E26L1N block cave, 9760RL, Drive end is towards cave edge, chainage 186.9 m. Approximately 10 m from the cave edge. Shear crack mapping indicates the cave edge moving down relative to solid ground and is marked in green; (b) Extraction drive 8, E26L1N block cave, 9760RL, end of drive length, chainage 181 m. Approximately 15 m from the cave edge. Photos 4 and 5 in reference location Figure 5

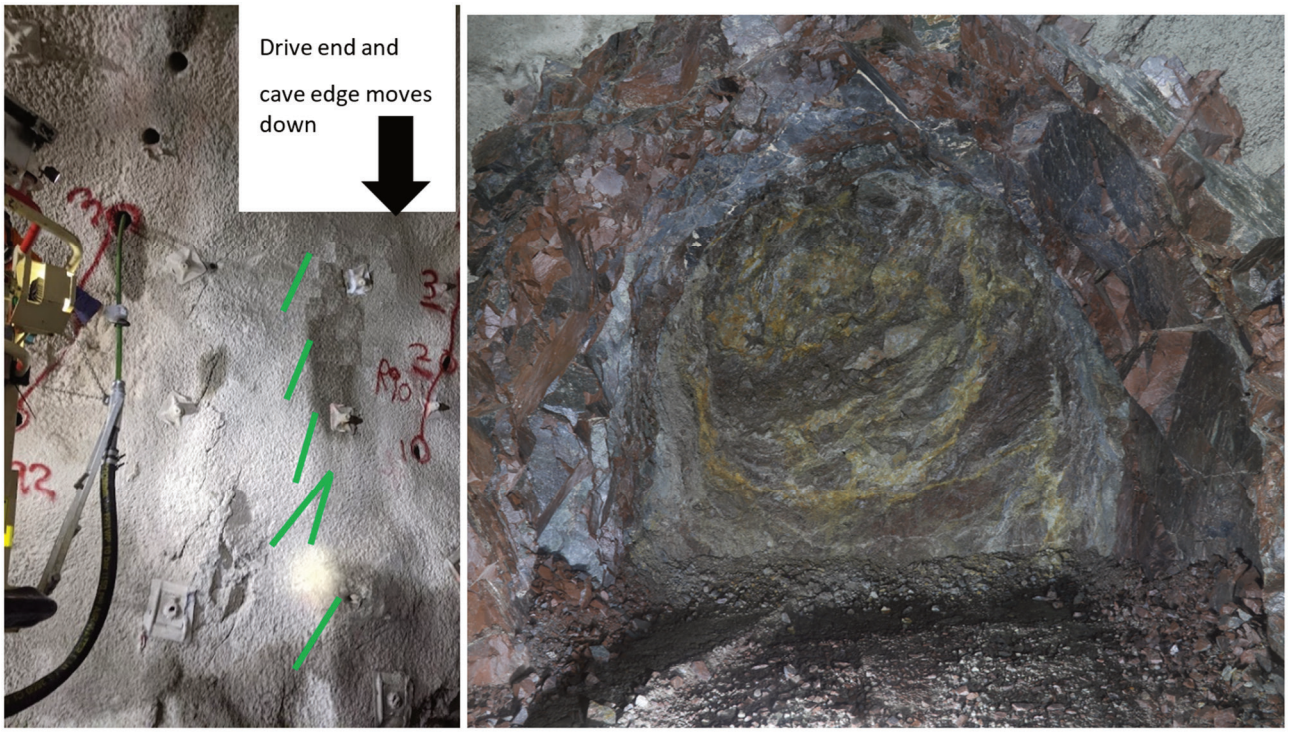

(a) (b)

Figure 14 (a) Shear cracks seen in undercut drive 8, E26L1N block cave, 9780RL. Drive end and cave edge is to right side of photo. Shear crack mapping indicates the cave edge moving down relative to solid ground. Photo 6 in reference location Figure 5; (b) Drill drive seven in the E26L1N undercut, end of drive. The rock mass at the face is oxidised on fracture surfaces indicating air and water conductivity is greater here than the rock seen in the side walls and roof. Photo 7 in reference location Figure 5

2.6 Summary of underground observations

From the observations and measurements taken from the cave edge drives and drill holes, the following can be summarised:

- Tensile strain at the cave edge is observed as tensile opening and increase of aperture of existing discontinuities.
- Shear movement at the cave edge is observed where the edge can move vertically downwards.
- Strain around the cave zone is accommodated on discrete discontinuities and between these discontinuities, the rock mass maintains its original integrity. There is no overall loosening of the rock mass or a gradual increase in loosening towards the cave edge.
- New fractures are seen in areas of the cave back where preconditioning (blasting) was performed in the past to promote caving. These are not seen in cave edges where preconditioning was not performed. They may exist in the 'crown' of the cave as it grows vertically; however, these were not encountered in development.
- Water flow on structures is focused in individual structures rather than throughout a network of connected paths.
- From the stress modelling and seismicity monitoring, the open discontinuities mapped represent the failed zone of the cave edge. Here, the material between the cave edge and the failure plane is yielded and no longer sustaining high loads.

3 Coupled triaxial and X-ray computer tomography experiment

XCT techniques have enabled non-destructive observations of the inner structure of materials, and advancements in reconstruction techniques have resulted in high-resolution and high-quality images of more dense materials, including hard rock (Cnuddle & Boone 2013). This technology has a long history in the oil and gas industry; however, applications to hard rock mining are developing. For example, XCT allows a three-dimensional image to be produced of rocks that previously could only be observed from the rock surface. In addition, the tomogram can be interrogated in a variety of software to achieve precise 3D calculations of the material structure.

An experimental project has been designed with the Australian National University and Beck Engineering to apply XCT to a mechanical strength experiment. The coupling of XCT and laboratory experiments enable the fracture mechanics to be imaged, measured and registered between the loading stages of the test. The first experiment demonstrates that the coupled triaxial cell and imaging can be successfully performed on an inhomogeneous, hard rock.

3.1 Experiment design

The Australian National University triaxial cell is located on a stage within the XCT, enabling the sample to be imaged in situ while under triaxial load (Figure 15). In addition to the coupled triaxial cell and µCT, the apparatus is instrumented to allow the continuous monitoring and data acquisition of axial and confining pressure and displacement throughout the stages of the experiment. The rock sample tested in the coupled XCT, and the triaxial cell was 23 mm in diameter and 78 mm in length. The rock type is monzonite from the gypsum leach zone of the deposit, where the strength is reduced compared to the fresh sample. This reduced strength was desirable to ensure it would fail with the capacity of the apparatus. The sample contains open fractures and pores due to the leaching process that removed gypsum veining.

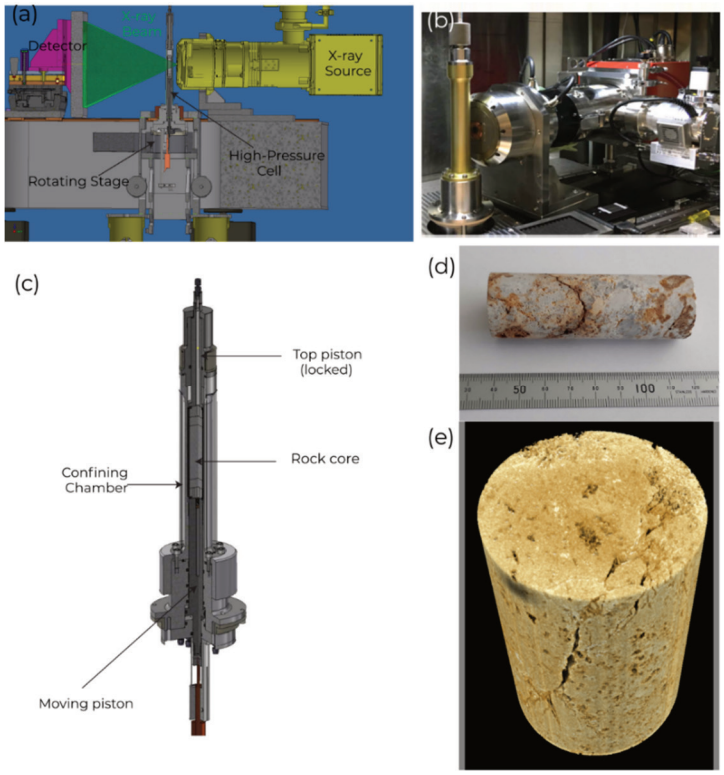

Figure 15 (a) Computer-aided design drawings of the apparatus setup with µCT imaging of the high-pressure cell and rotating stage; (b) Photograph of the X-ray source aligned against the high-pressure cell on left; (c) Schematic of the main component of the high-pressure, triaxial cell with the sample location; (d) 23 mm diameter sub-core used in this experiment. (e) Oblique view of the processed tomogram of the sample showing fractures after failure

3.2 Experimental results

The coupled experiment successfully produced nine high-resolution images throughout the loading stages of the experiment through to failure. Analysis of the images allows the three-dimensions of the micro-mechanisms within the sample to be observed clearly illustrating the stages of brittle failure. The tomogram images are shown as two-dimensional slices in Figure 16 where the first image (before loading) and ninth image (after failure) are shown with the sample encapsulated in place within the triaxial cell. The experiment failed in a brittle manner through the top of the sample, on a 45° fracture. Bieniawski (1967) describes the failure stages as fracture closing, new fracture nucleation, and fracture coalescence, and these can be identified within the tomograms. Figure 17 contains four of the nine tomogram images collected during the triaxial loading stages of the porphyry rock. This laboratory experiment is a different scale and geometry to a propagating cave; however, the sequential tomograms enable the 3D observations to be registered to calculate the strain map of the sample and the complex failure path extracted from the sample.

The XCT tomography resolution to nine microns shows the loading of the sample is taken up in the closure of existing fractures of the rock. As the experiment continues, these fractures coalesce with other fractures until the sample reaches instability and shear failure breaks through intact parts of the sample. Prior to failure, the damage to the sample is constrained to the fracture planes that partition undamaged material. With the mobilisation of the failed block, between the initial fracture paths, smaller rock fragments form as the sample begins to comminute.

The existing fracture forms the main path for any water flow in the sample. As load is applied to the sample, the aperture decreases, reducing conductivity through the sample. The continual loading extends and initiates new fractures creating new pathways of conductivity. As the sample fails, the fractures connect, and the main fracture moves in shear, increasing the aperture again. This non-linear trend of conductivity with strain can be visualised in the tomograms.

Collecting high-resolution images on dense materials coupled with experimental apparatus is an involved laboratory experiment. However, the mass of data documenting the experiment provides a valuable understanding of fracture spacings, multiple failure mechanisms, and their interactions to improve geomechanical modelling. Additionally, the ability to register particles between stages (Saadatfar et al. 2012) shows the opportunity further to design experiments for cave comminution and flow mechanisms.

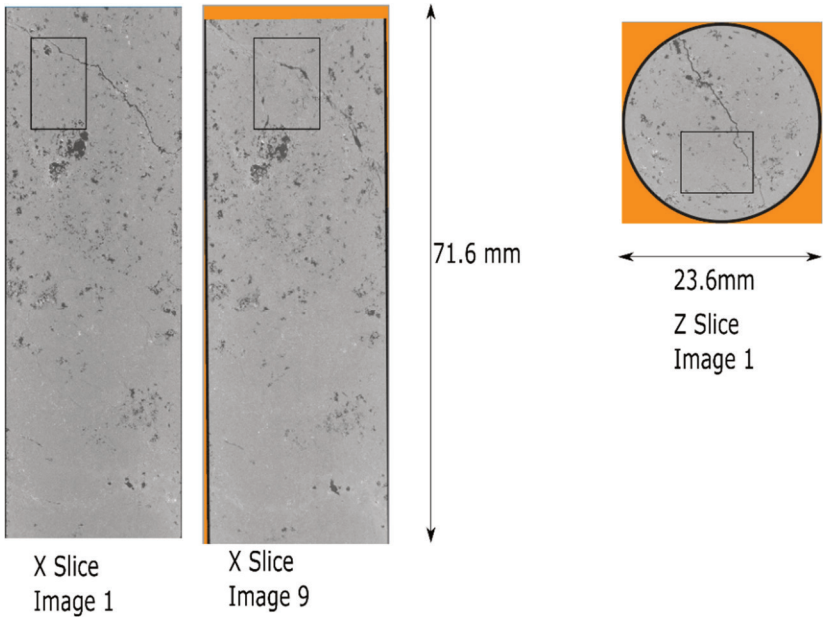

Figure 16 Tomogram images of the porphyry sample from the coupled triaxial experiment. X orientation slices through the sample tomogram at the beginning (image 1) and end of the experiment (image 9). Z slice from the beginning of the experiment. The rectangle marked on the slices is the location of the subset in Figure 17

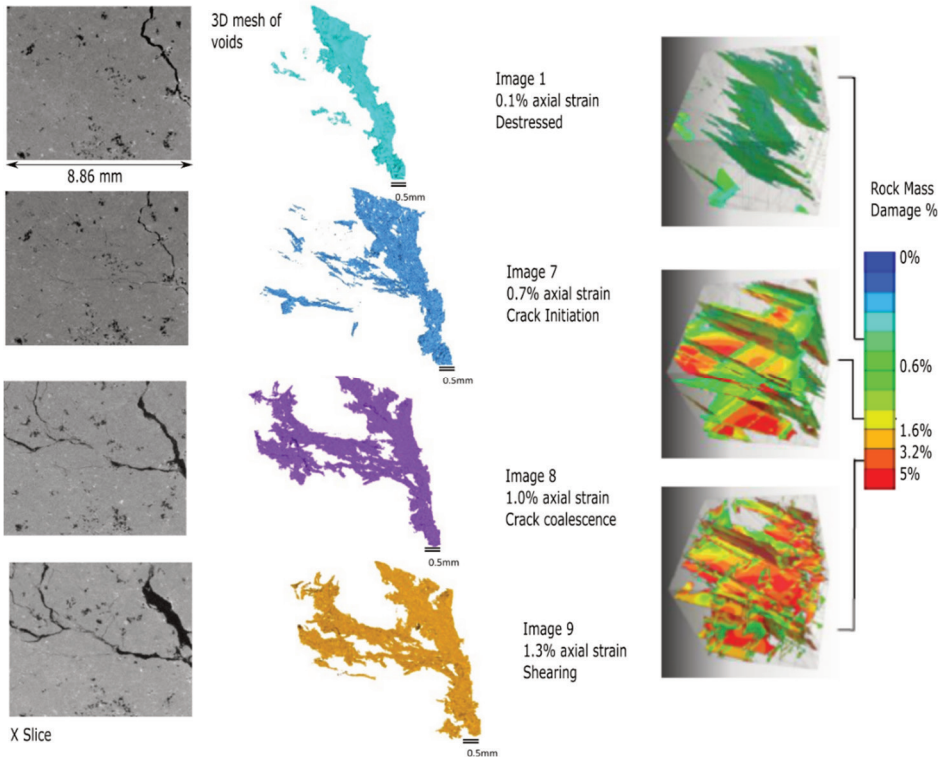

Figure 17 Subsample extract of sheared portion from the coupled XCT and triaxial experiment. The left images are the four tomograms from the experiment (images 1, 7, 8 and 9). The second column shows the extracted mesh surfaces from the void portion of the tomogram (Webster et al. 2022). For reference, the magnitude of plastic deformation is shown correlating to the damage in a microscale discontinuum planes (Beck 2013; Flatten et al. 2016)

4 Learnings from underground and experimental observations

Considering the observation and modelling from the Northparkes cave edge mining with the XCT 3D imaging experiment, the below observations are made regarding strain and conductivity in heterogenous, hard rocks:

- Moderate stress increases underground and in the loading of the rock specimen present as the reduced aperture of existing discontinuities.
- Strain around the cave zone and in the rock specimen is accommodated on discrete discontinuities and between these discontinuities the rock maintains its original integrity until the stage of unstable fracture propagation.
- There is no overall loosening of the rock mass or a gradual increase in loosening towards the cave edge.
- Localised discontinuities display surface oxidation and copper oxide secondary mineralisation, indicating a connection to the cave or surface. Surrounding discontinuities are not stained indicating conductivity is concentrated within isolated pathways rather than the rock mass acting as a porous media or network of fractures.
- Blocks defined by discontinuities that fail begin to fragment as confinement is lost. Further comminution occurs with rotation in shearing mechanisms.
- Regular spacing was not observed in discontinuities opening in tension in the cave edge development.
- Conductivity decreases through the closing of apertures when stress is applied to the rock mass (through mining or in the experiment).

- Conductivity increases with damage in the form of relaxation, fracture propagation or shearing on discontinuities.

5 Conclusion

This paper shows the mine examples of how the ground conditions contain discrete discontinuities accommodating for the damage around remnant caves. These discontinuities containing evidence for groundwater support the understanding that in hard rock, most groundwater flows through localised discontinuities and the importance of understanding the evolution of rock mass damage and the associated changes in conductivity.

The coupled XCT mechanical tests demonstrate the 3D evolution of damage on a discontinuity with increasing strain on the sample. The imagery shows the conductivity decreasing as the rock strain is taken up through closure of fracture apertures then with further strain, conductivity increases again as new flow paths form and shearing causes dilation of the rock.

This work progresses the understanding of the interaction of caving operations and groundwater to improve the quality of forecasting the coupled rock mass and hydrology response. The experiments focused on non-linear trend of conductivity with strain will be progressed to further define and improve the modelling interactions.

Acknowledgement

The authors thank the reviewers for their constructive comments on this paper, CMOC Northparkes Mines, for the opportunity to publish this work, Beck Engineering, and The Australian National University Department of Material Physics for their contributions to the experiment and project.

References

Beck, D 2017, *Letter Regarding E26L1N Layout*, Beck Engineering unpublished report, Beck Engineering, Sydney.

Bieniawski, ZT 1967, 'Mechanism of brittle fracture of rock: Part I—theory of the fracture process', *International Journal of Rock Mechanics and Mining Sciences & Geomechanics Abstracts*, vol. 4, issue 4, pp. 395–406.

Cnudde, V & Boone, MN 2013, 'High-resolution X-ray computed tomography in geosciences: a review of the current technology and applications', *Earth-Science Reviews*, vol. 123, pp. 1–17.

Duplancic, P & Brady, BH 1999, 'Characterisation of caving mechanisms by analysis of seismicity and rock stress', *Proceedings of the 9th International Congress on Rock Mechanics*, vol. 2, A.A. Balkema, Rotterdam, pp. 1049–1053.

Flatten, A, Reusch, F & Beck, D 2016, 'The application of hydromechanical mine-scale modelling for large block caving operations', *MassMin 2016: Proceedings of the Seventh International Conference and Exhibition on Mass Mining*, The Australasian Institute of Mining and Metallurgy, Melbourne, pp. 341–348.

Read, J & Stacey, P 2009, *Guidelines for Open Pit Slope Design*, CSIRO Publishing, Clayton South.

Ross, I & van As, A 2005, 'Northparkes mine – design, sudden failure, air blast and hazard management of the E26 Block Cave', *Proceedings of the 9th Underground Operators Conference*, Australia, Australasian Institute of Mining and Metallurgy, Melbourne, pp. 7–21.

Saadatfar, M, Francois, N, Arad, A, Madadi, M, Cruikshank, R, Alizadeh, M, Sheppard, A, Kingston, A, Limay, A & Senden, T 2012, '3D mapping of deformation in an unconsolidated sand: a micro mechanical study', *SEG Technical Program Expanded Abstracts*, Society of Exploration Geophysicists, Houston.

Talu, S, van As, A, Seloka, W & Henry, R 2010, 'Lift 2 North extension cave performance', in Y Potvin (ed.), *Caving 2010: Proceedings of the Second International Symposium on Block and Sublevel Caving*, Australian Centre for Geomechanics, Perth, pp. 407–421,

Umar, S 2017, *Caving Mechanisms for a Non-Daylighting Orebody*, PhD thesis, Luleå University of Technology, Luleå.

Webster, S, Samosir, E & Wyllie, A 2020, 'Learnings from mining cave extensions at Northparkes Mines and new technology to improve the value of future cave designs', in R Castro, F Báez & K Suzuki (eds), *MassMin 2020: Proceedings of the Eighth International Conference & Exhibition on Mass Mining*, University of Chile, Santiago, pp. 92–102, doi.org/10.36487/ACG_repo/2063_01

Webster, S, Saadatfar, M & Francois, N 2022, *Coupled Micro-Computer Tomography and Micromechanical Experiment on the Brittle Failure of Porphyry Sock*, unpublished manuscript, The Australian National University, Department of Material Physics.